Solid State Ionics 321 (2018) 69–74

Contents lists available at ScienceDirect

Solid State Ionics

journal homepage: www.elsevier.com/locate/ssi

Charge carrier chemistry in methylammonium lead iodide

Alessandro Senocrate[a,b], Tae-Youl Yang[a,1], Giuliano Gregori[a], Gee Yeong Kim[a], Michael Grätzel[a,b], Joachim Maier[a,*]

[a] Max Planck Institute for Solid State Research, Heisenbergstr. 1, 70569, Stuttgart, Germany
[b] Department of Chemistry and Chemical Engineering, Swiss Federal Institute of Technology (EPFL), Lausanne CH-1015, Switzerland

ARTICLE INFO

Keywords:
Ion migration
Perovskite solar cells
Methylammonium lead iodide
Ionic charge carriers
Electronic charge carriers

ABSTRACT

Both electronic and ionic transport properties are key issues in the performance of perovskite solar cells. In order to understand the electrical behavior of organic-inorganic halide perovskites, and the possibilities to influence them, the elucidation of their equilibrium charge carrier chemistry as a function of stoichiometry and dopant concentration is a necessary and fundamental prerequisite. We provide here insight into the point defect chemistry of methylammonium lead iodide, whereby the decisive carriers are identified and their concentrations discussed as a function of stoichiometry (iodine partial pressure) and dopant content (oxygen partial pressure or Na addition). The experimental results indicate how ionic conductivity, which can be attributed to iodine vacancies, and electronic conductivity, which can be attributed to electron holes (or conduction electrons under reducing conditions), can be significantly and systematically altered by such treatments. Experimental results are discussed in the context of simple defect chemical models.

1. Introduction

The discovery of the extraordinary performance of methylammonium lead halides (in particular of the iodide, here abbreviated as $MAPbI_3$) as photo-absorbers in all-solid-state dye-sensitized solar cells has led to intensive worldwide activities [1,2]. Since then, the electronic properties of these materials, that are of unquestionable importance for the solar function, have been extensively explored [3–5], while their ionic conductivity has been investigated only recently in a systematic manner [6–8]. These experiments, in agreement with some recent reports, show iodine to be very mobile [9–15]. As far as iodine defects are concerned, despite some computational studies [5,16] having reported low formation energies for interstitial defects, major emphasis should be given to vacancies (Schottky defect pairs) [17], due to the ease of formation that such defects commonly have in the dense perovskite structure. Mobility of the methylammonium cation has also been referred to in studies applying illumination and high bias and focusing on surface effects [15,18,19]. In agreement with NMR [8] and electrochemical [6] studies published earlier, as well as theoretical modeling [9], the effects of iodine partial pressure on the ionic conductivity (shown below) clearly indicate that methylammonium vacancies cannot be the predominant charge carrier shouldering the bulk conduction process at least under dark conditions. All this is not surprising and conforms with the well-known result that similar compounds such as $CsPbBr_3$, $CsPbCl_3$, $KMnCl_3$ [20] and $MAGeCl_3$ [21,22] are all halide conductors with comparable absolute values for conductivity and activation energies [6,20–22]. Independently of its nature, such a mixed ionic-electronic conductivity leads to bulk stoichiometry polarization whenever the perovskite is electrically biased while sandwiched between neighboring phases which are blocking for the ions, as it is the case in solar cell devices. This effect provides a straightforward explanation for the long time/low frequency “anomalies” reported in devices under operation, such as high “dielectric constant” [23] and hysteresis in *i*-V sweep experiments [24]. The bulk nature of these polarization phenomena has been supported by several studies, which reported on the formation of *p-i-n* junctions under load seizing the entire sample [18,19,25]. In contrast, other works discussing the consequence of ion conductivity in halide perovskites considered only the occurrence of a space charge polarization at the contacts [14,26–28]. While this process will surely also occur [29,30] - and may be relevant for charge carrier separation - space charge relaxation times are typically much smaller owing to the smaller capacitances involved and cannot explain the low frequency anomalies, at least not in thicker films [6,7]. Furthermore, ion transport is a crucial issue as far as the degradation kinetics of these rather unstable materials is concerned. The aim of the present paper is to elucidate the charge carrier chemistry (point defect chemistry) in methylammonium lead iodide, where this does not only address the nature of the point

* Corresponding author.
E-mail address: s.weiglein@fkf.mpg.de (J. Maier).
[1] Present address: Korean Research Institute of Chemical Technology, 141 Gajeong-ro, Yuseong-gu, Daejeon, Korea.

https://doi.org/10.1016/j.ssi.2018.03.029
Received 17 January 2018; Received in revised form 23 March 2018; Accepted 28 March 2018
Available online 13 April 2018

defects involved but also their dependence on the degrees of freedom (such as temperature, stoichiometry, impurity and doping content). Through purposeful tuning of these degrees of freedom we will show that both ionic and electronic conductivities, respectively attributed to iodine vacancies and electron holes, can be severely modified. Here we want to stress once again that these considerations refer to equilibrium conditions and hence to the situation in the dark.

2. Results and discussion

A mixed conductor can exchange matter with the surrounding gas phase, therefore its charge carrier concentrations (and thus electronic and ionic transport properties) will depend not only on the temperature, but also on the outer partial pressure of every exchangeable component. Furthermore, its charge carrier chemistry is crucially influenced by impurities or dopants, if these concentrations are on the order of magnitude of the majority carriers. The impact of these parameters is not only critical for a detailed understanding of the material properties, but also reveals suitable adjusting screws to tune the electrical transport properties. To be precise, for a dilute, simple charge carrier chemistry one can show that the equilibrium concentration of any electronic and ionic charge carrier (j) can be given as

$$c_j(T, P_k, C) = \alpha_j \left(\prod\nolimits_r K_{rj}^{\gamma_{rj}}(T)\right) C^{M_j} \left(\prod\nolimits_k P_k^{N_{kj}}\right) \quad (1)$$

where the P_k's are the partial pressures of the reversibly exchangeable components ($k = I_2$, O_2, etc.), T is temperature and C is the effective dopant concentration [31,32]. The parameters α, γ, M, N are simple rational numbers and follow from solving the defect-chemical mass action problem [33,34]. These numbers change if the nature of the majority carriers changes and are hence characteristic for the specific defect regimes (highlighted by different capital letters in the defect diagrams of Figs. 1 and 2). Eq. (1) predicts an exponential T-dependence via the mass action constants K_r of reaction r, a power law behavior as regards P_k and a power law behavior as regards the doping content C. For the oxide perovskite $A^{II}B^{IV}O_3$ it is well established that, owing to the dense lattice, the major disorder reaction is the partial Schottky reaction leading to AO deficiency and hence to A and O vacancies (V_A'', $V_O^{\bullet\bullet}$) as majority defects. As oxygen vacancies are sufficiently mobile, the decisive partial pressure that can induce stoichiometry variations is the oxygen partial pressure (P_{O_2}). At sufficiently low P_{O_2}, the perovskite is n-type (excess electrons in B orbitals, forming B^{3+}) and at sufficiently high P_{O_2} p-type (holes in oxygen orbitals, yielding O^-), providing the stability limit is not exceeded. Similarly in $MAPbI_3$, valence and conduction bands are formed by I and Pb orbitals respectively [4,5], whereupon at low P_{I_2}, presumably extremely low P_{I_2}, we expect the material to be n-type (excess electrons predominantly in Pb orbitals, forming Pb^+) and at sufficiently high P_{I_2} p-type (holes predominantly in I orbitals, forming I^0). MA-interstitials and Pb-defects may also occur, but can be treated as frozen dopants (entering the C factor of Eq. (1)). Their effect on the defect chemistry can be neglected as long as their concentrations are not in the range of the majority carriers. Moreover, their mobilities are expected to be too low to influence the overall ion transports [9,10]. As mentioned, in $MAPbI_3$ iodine mobility is significant, while the mobility of MA^+ ions appears to be minor but possibly not negligible [6,9,19]. Hence the major control parameter in terms of electric transport is P_{I_2}, together with temperature and dopant content. The latter comprises frozen-in native defects as well as intentional or non-intentional impurities, all summing up (positively or negatively) in C.

Regarding the I_2 effect, this consists in decreasing the iodine deficiency (we ignore here the possible occurrence of I-excess) according to:

$$\frac{1}{2}I_2 + V_I^{\bullet} \rightleftharpoons I_I^x + h^{\bullet} \qquad K_I = \frac{[h^{\bullet}]}{[V_I^{\bullet}]P_{I_2}^{1/2}} \quad (2)$$

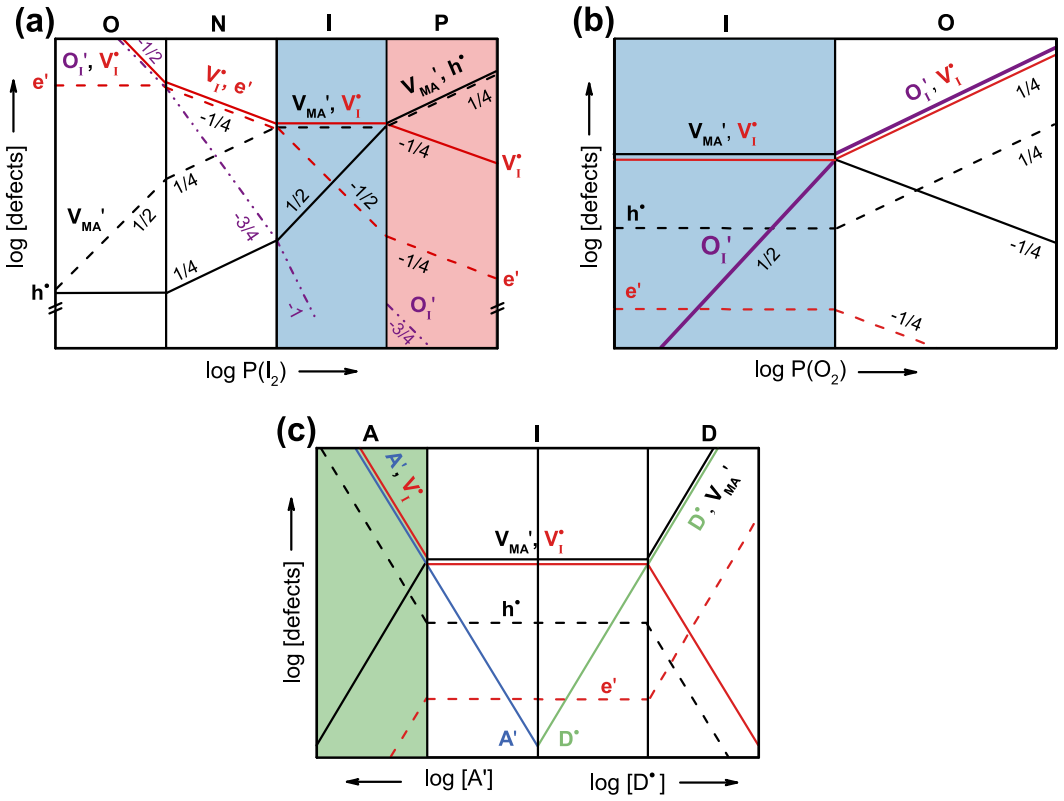

Fig. 1. Kröger-Vink diagrams of undoped $MAPbI_3$ as a function of **(a)** I_2, **(b)** O_2 partial pressures (also given in Ref. [35]), **(c)** doping content. The capital letters on the abscissas indicate different transport regimes depending on the majority mobile carriers dominating: excess electron holes (P), intrinsic (I), excess electrons (N), oxygen-dominated (O), acceptor doped (A), donor doped (D). The slopes for the various defect concentration are given directly on the figure.

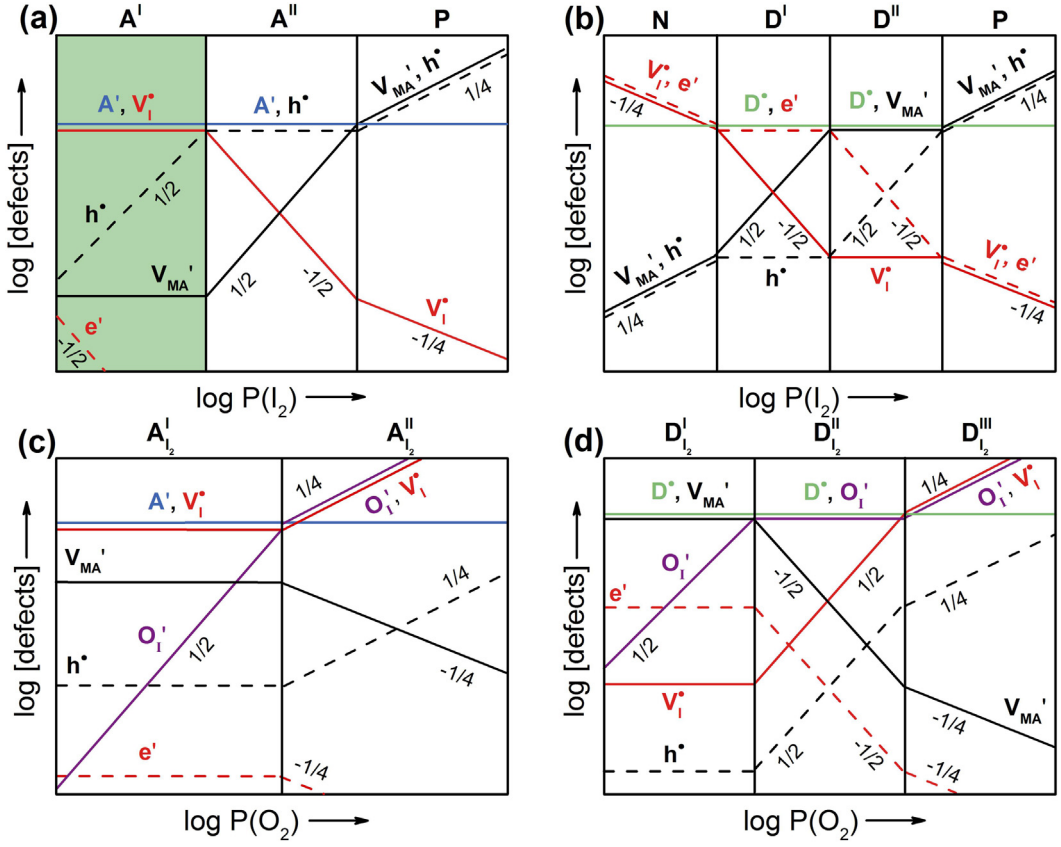

Fig. 2. Kröger-Vink diagrams calculated as a function of I_2 and O_2 partial pressure for **(a)**, **(c)** acceptor- and **(b)**, **(d)** donor-doped $MAPbI_3$. The slopes for the various defect concentration are given directly on the figure.

Also oxygen incorporation needs to be taken into account, since oxygen can replace iodine leading to a $O_I^{'}$ defect [35]. Therefore, on a time scale on which

$$\frac{1}{2}O_2 + V_I^{\bullet} \rightleftharpoons O_I^{'} + 2h^{\bullet} \qquad K_O = \frac{[h^{\bullet}][O_I^{'}]P_{I_2}^{1/2}}{P_{O_2}^{1/2}} \tag{3}$$

is reversible, oxygen has to be considered as an exchangeable component and P_{O_2} enters the P_k-term, otherwise $[O_I^{'}]$ can be treated as an impurity and enters the C-term as a constant (see Eq. (1)). From the mass action laws of the defect equations previously presented, together with the electroneutrality equation, we can derive the relevant defect diagrams (known as Kröger-Vink diagrams) for $MAPbI_3$, as shown in Fig. 1. For simplicity, we do not consider lead defects, nor iodine and methylammonium interstitials in the model. However, we note that they would not change the picture as long as they are not predominant, and even in the case in which they would intrinsically compensate iodine vacancies, this would not change the major operative conclusions (see Supporting Information for a detailed discussion). Fig. 1a shows the concentrations of iodine vacancies, methylammonium vacancies, excess electrons and electron holes as a function of iodine partial pressure. This diagram has been plotted considering a fixed O_2 partial pressure and it also allows for a small concentration of equilibrium substitutional oxygen defects (only relevant at very low P_{I_2}). Qualitatively one recognizes that the hole concentration $[h^{\bullet}] \equiv p$ is expected to increase with P_{I_2}, while the opposite holds for $[e'] \equiv n$. The iodine vacancy concentration is predicted to decrease with P_{I_2} (at constant T, P_{O_2}), while an opposite trend is expected from V_{MA}'. Considering oxygen exposure, Fig. 1b presents the defect diagram of $MAPbI_3$ as a function of P_{O_2}, calculated for conditions under which Eq. (3) is reversible and under constant P_{I_2}. Here, both the electron hole concentration and the iodine vacancy concentration are expected to increase with P_{O_2}, while $[e']$, $[V_{MA}']$ will behave oppositely. We note that for the majority carriers dominating the electroneutrality equation, such changes are generally small and negligible (relatively speaking, on log scale), but they are significant (again, on log scale) for the minority species.

Accordingly, in both defect diagrams obtained as a function of P_{I_2} and P_{O_2}, in the intrinsic (I) region the majority carriers show flat profiles (slope = 0), while the slopes of the minority carriers are significant (given as labels in the figures). As far as the doping effect is concerned, the relevant defect diagram is shown in Fig. 1c; here, acceptor addition is expected to increase $[h^{\bullet}]$, $[V_I^{\bullet}]$, (and to decrease $[e']$, $[V_{MA}']$), while the opposite will naturally occur on donor doping. As for a pure sample, it is possible to calculate defect diagram as a function of P_{I_2} and P_{O_2} also for acceptor- and donor-doped $MAPbI_3$. These are given in Fig. 2.

We have now obtained a clear picture of how the point defect (charge carrier) concentrations in $MAPbI_3$ are expected to behave as a function of several parameters. We can thus confirm these predictions by measuring the ionic and electronic conductivities of $MAPbI_3$ as a function of the aforementioned control parameters. The conductivity measurements are carried out by means of DC-galvanostatic polarization using ion-blocking electrodes (that allows us to separate the electronic and ionic contributions) [36] as a function of iodine partial pressure, oxygen partial pressures and dopant content. By assuming mobility values to be constant with respect to P_{I_2}, P_{O_2} or doping, we can relate defect concentrations with conductivity values and therefore directly compare defect chemical considerations and experiments.

Firstly, we consider the conductivity variation as a function of iodine partial pressure (Fig. 3a) for an undoped $MAPbI_3$ sample. The increase of σ_{eon} indicates p-type electronic conductivity, in agreement with our previous report [6,8]. The decrease of σ_{ion} indicates ion conductivity via iodine vacancies as predicted by Fig. 1a. Note that a conductivity process due to methylammonium vacancies would behave oppositely. The measured slopes are found between the values expected

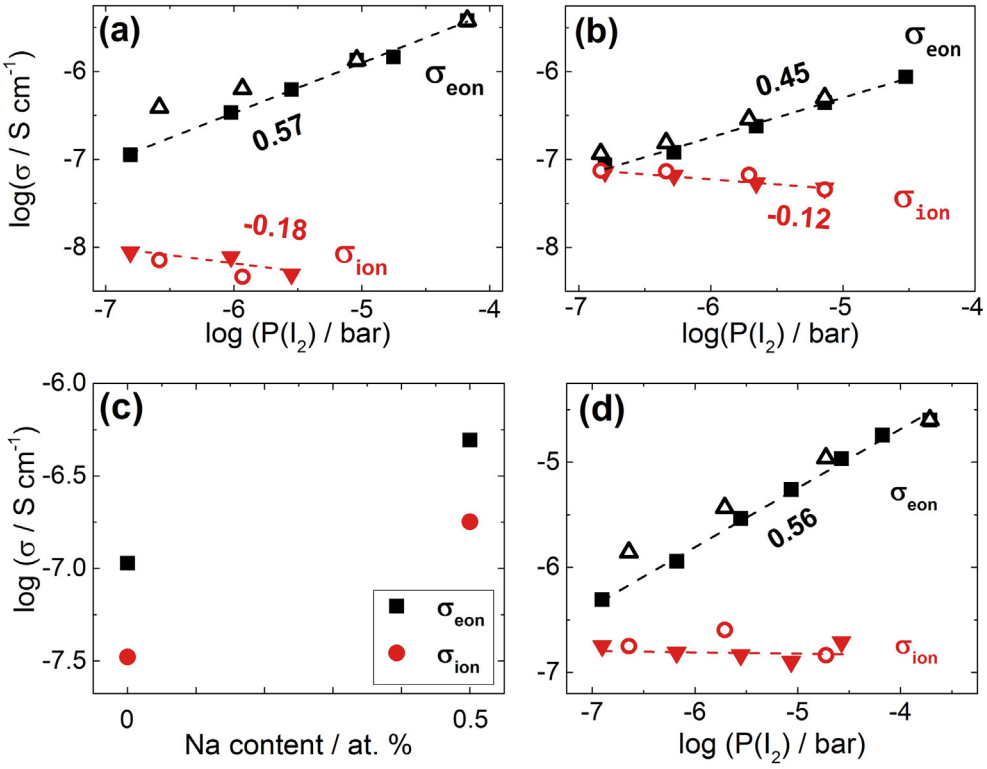

Fig. 3. De-convoluted ionic and electronic conductivities of undoped $MAPbI_3$ as a function of P_{I_2} (carrier gas = Ar, $P_{O_2} = 10^{-4.5}$ bar), measured at **(a)** 70 °C and **(b)** 105 °C. Data were recorded from low to high partial pressure (solid symbols, ■ eon, ▼ ion) and then from high to low (open symbols, △ eon ◁ ion) to observe reversibility. **(c)** Comparison between the conductivity of undoped and 0.5 % Na-doped $MAPbI_3$ **(d)**. **(d)** Iodine partial pressure dependence of the conductivity measured for a Na-doped sample (0.5 % at.). Again, reversibility was observed recording the dependence from high to low partial pressure (open symbols). In all the above panels, the numbers given are the slopes of the linear fit represented by the dashed lines.

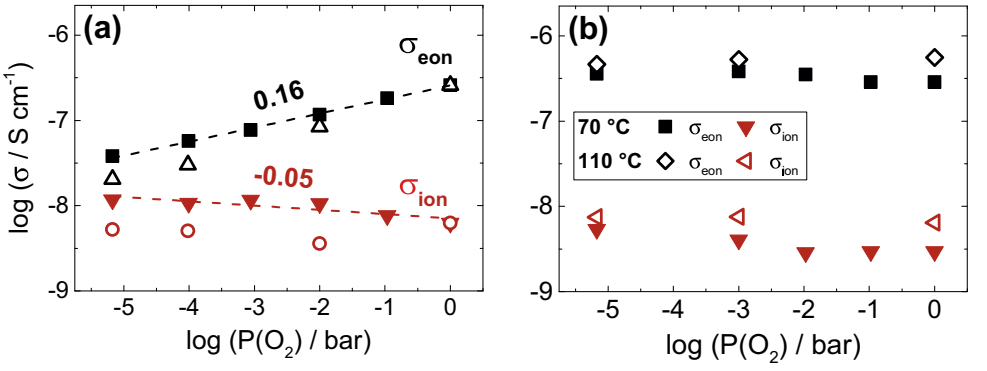

Fig. 4. (a) P_{O_2} dependence of the conductivity (carrier gas = Ar, P_{I_2} = unknown) at 70 °C for undoped $MAPbI_3$. Data were recorded from low to high partial pressure (solid symbols, ■ eon, ▼ ion) and then from high to low (open symbols, △ eon ◁ ion) to observe reversibility. The numbers given are the slopes of the linear fit represented by the dashed lines. **(b)** P_{O_2} dependence of the conductivity of undoped $MAPbI_3$, this time recorded under constant P_{I_2} (carrier gas = Ar, $P_{I_2} = 10^{-5.3}$ bar), both at 70 °C (solid symbols, ■ eon, ▼ ion) and 110 °C (open symbols, ◊ eon ◁ ion).

for I and P regimes of the related Kröger-Vink diagram (Fig. 1a) and indicate transition from intrinsic disorder to the iodine excess regime. The true error margins for the slopes might be perceptible due to the ambiguity in the determination of the true iodine partial pressure (as reported in Supporting Information), but this would not change our semi-quantitative conclusions. The occurrence of a P regime is not in contradiction with our previous report of overwhelming ionic defect concentrations as they referred to conditions of very low P_{I_2} [6]. It should also be noted that the boundaries of the defect chemical regimes depend also on the intrinsic level of MAI-deficiency and hence on the synthesis procedure and thermal history. Nevertheless, we recognize that, in $MAPbI_3$, the defect situation is expected to be dominated by ionic defects [17], in agreement with electrical measurements in the dark showing comparable σ_{ion} and σ_{eon} (normally one expects $u_{ion} \ll u_{eon}$). Even though the variation of $\log(\sigma_{ion})$ with $\log(P_{I_2})$ is small, it still shows a noticeable decrease that indicates that the ratio of ionic and electronic carrier concentration is not as large as anticipated (corresponding to the transition between I- and P-regimes). If this is indeed the case, then the ratio u_{eon}/u_{ion} must be smaller than expected. One possibility is a rather low u_{eon} in the dark, notwithstanding the fact that under illumination, u_{eon} (10–100 $cm^2 V^{-1} s^{-1}$) [37,38] is significantly larger than u_{ion} (10^{-7}–10^{-9} $cm^2 V^{-1} s^{-1}$) [8,15]. The second possibility is a severe underestimation of the reported ionic carrier mobility.

Let us now refer to the doping experiments (defect diagram in Fig. 1c). By inserting Na into the structure, a substitutional defect of Na on the Pb-site is generated (Na_{Pb}'), which is effectively negatively charged (acceptor doping). Thus, the dopant must be compensated by an increase in the concentration of positive defects, and a decrease of negative ones. Generally, this compensation occurs both electronically and ionically, with the individual changes being determined by the mass action laws. For $MAPbI_3$, we expect an increase of both ionic ($V_I^{\bullet}$) and electronic ($h^{\bullet}$) conductivity, and this is indeed observed as reported in Fig. 3c. In addition, the conductivity slopes as a function of P_{I_2} (Fig. 3b) are in agreement with the expected Kröger-Vink diagram of Fig. 2a (section A_1).

The P_{O_2} behavior is very intriguing as well. Fig. 4a displays an increase of the electronic conductivity as qualitatively expected for O-incorporation, but an ionic behavior that is fairly constant (or slightly decreasing), in contrast with what is expected from Fig. 1b. Rather the

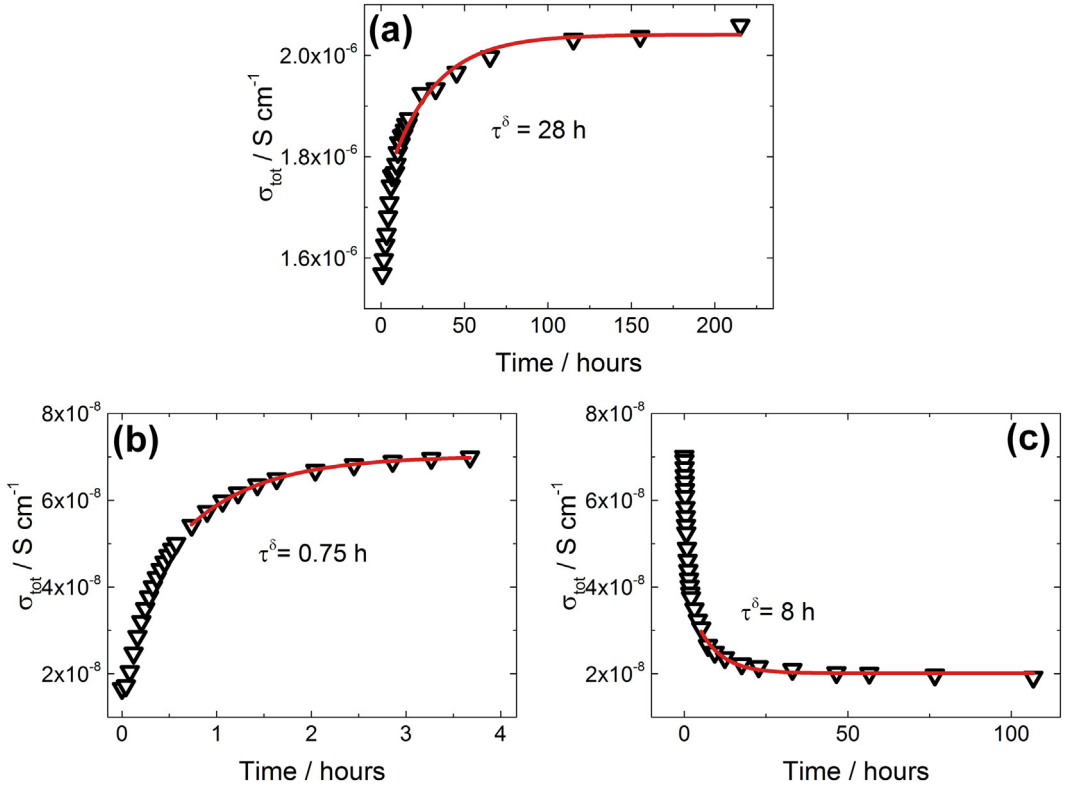

Fig. 5. Conductivity equilibration of undoped $MAPbI_3$ after changing **(a)** P_{I_2} from 10^{-7} to $10^{-6.2}$ (carrier gas = Ar, $P_{O_2} = 10^{-4.5}$ bar, T = 70 °C), **(b)** P_{O_2} from $10^{-5.1}$ to 10^{-3} bar (T = 70 °C, carrier gas = Ar, P_{I_2} unknown) and **(c)** P_{O_2} (reverse) from 10^{-3} to $10^{-5.1}$ bar (T = 70 °C, carrier gas = Ar, P_{I_2} unknown). Solid lines represent exponential fits of the equilibration times. The extracted time scales (τ^{δ}) are given on the figure.

situation is qualitatively similar to the I_2-effect. Let us stress again that all the σ_{ion} and σ_{eon} variations upon changes in P_{I_2} or P_{O_2} show a satisfactory reversibility.

Interestingly, as shown in Fig. 5a, upon exposing a sample to I_2 partial pressure we observe a rather long equilibration time (τ^{δ} (I_2) = 28 h) for the conductivity, while the apparent equilibrium on P_{O_2} increase is much faster (Fig. 5b, τ^{δ} (O_2) = 0.75 h). Also, the time constant upon reversing P_{O_2} is again distinctly longer (Fig. 5c). All this speaks for a surface effect in which O_2 oxidizes the sample surface, providing an enhancement of the iodine activity. Indeed, if P_{I_2} is constant ($10^{-5.3}$ bar), one observes invariant σ_{ion} and σ_{eon} values (Fig. 4b). Increasing the temperature to 110 °C does not influence the situation, ruling out the possibility that slow kinetics might prevent conductivity changes to be observed during the time scale of the measurements (even though we wait for several days between any two subsequent points). In view of the rapid O_2-effect, it appears that O_2 treatment leads to a kinetically determined variation of the iodine activity more rapidly than the I_2 interaction itself. This is not unexpected, since at room temperature it is frequently the surface reaction (here $I_2 \rightarrow I^{-}_{surface}$), and not the bulk diffusion step, that is rate determining in a chemical exchange [39]. This interesting phenomenon will be analyzed in more detail elsewhere [35]. There, it is also shown how in $MAPbI_3$ the oxygen incorporation can be quickly enhanced by illumination, whereupon it results in an expected doping effect if the oxygen partial pressure is taken sufficiently high (Fig. 1b, section O). Thermodynamically, this feature corresponds to the oxygen content changing its role from an in-situ to an ex-situ parameter, as discussed in Ref. [40].

3. Conclusions

In summary, the present contribution provides a defect chemical interpretation of conductivity results obtained on $MAPbI_3$ as a function of different control parameters such as iodine and oxygen partial pressures, and dopant content. As expected, the relation between cationic, anionic and electronic defects (as well as their dependence on the surrounding atmosphere) is rather similar to the situation in other better known perovskites. $MAPbI_3$ is evidently a pronounced mixed conductor under equilibrium conditions, as proven by the severe stoichiometric bulk polarization observed under load. Analogously to oxide perovskites, ion migration appears to be dominated by anion vacancies. Furthermore, this work shows how electric transport properties can be significantly tuned by varying several control parameters. The effects are found to be at least in semi-quantitative agreement with the idealized defect chemical predictions. Interestingly, exposing $MAPbI_3$ to oxygen under equilibrium seems to trigger a higher I-activity, which is suggestive of rather complex surface reaction. These findings are relevant for a full understanding of the seemingly elusive charge carrier chemistry in $MAPbI_3$, which is an indispensable prerequisite for precisely defining the electrical behavior of the material and, most importantly, its photovoltaic performance.

4. Experimental details

4.1. Synthesis

MAI was obtained using the reported procedure by Im et al. [41] The synthesis of $MAPbI_3$ samples was carried out according to the procedure by Saidaminov et al. [42] Single crystals were obtained by heating to 125 °C a 1 M solution of PbI_2 (Alfa Aesar, 99.9985%, metals basis) and MAI (1:1) for 3–4 h, with no stirring. In the case of Na-doped samples, NaI was added to the solution in order to obtain PbI_2:NaI:MAI ratio as 0.99: 0.01: 1. After heating, the remaining solution was removed and the crystal dried under rough vacuum (around 10 mbar) at room temperature for several hours. The synthesis step was carried out in normal laboratory atmosphere. Phase purity was assessed with XRD (Fig. S1).

4.2. Pellet preparation

The as-obtained crystal (0.1–1 mm size) were subsequently transferred into a glovebox, ground in a mortar and cold pressed at 5–7 kN in a 5-mm diameter pellet (final thickness of 0.6–0.7 mm). Graphite foil (Alfa Aesar, 99%, 0.4 mm thickness) was placed below and above the powders prior to the pressing step, in order to create graphite electrodes. Relative density of the pellets was around 95%.

4.3. DC-galvanostatic polarization

DC polarization experiments were conducted by using a current source (Keithley model 220) and by monitoring the potential change with an electrometer (Keithley model 6514). Measurements were carried out in the dark and in a gas-tight quartz tube placed in a tube furnace. Details on atmosphere control are reported in the Supporting Information.

Notes

The authors declare no competing financial interests.

Acknowledgments

The authors would like to thank Dr. Helga Hoier for performing XRD measurements and Dr. Rotraut Merkle for very helpful discussions and suggestions. This work was performed within the framework of the Max Planck-EPFL Center for Molecular Nanoscience and Technology.

Appendix A. Supplementary data

XRD data, experimental details on atmosphere control and considerations on chemical diffusion and defect chemistry are found in the Supporting Information. Supplementary data to this article can be found online at https://doi.org/10.1016/j.ssi.2018.03.029.

References

[1] A. Kojima, K. Teshima, Y. Shirai, T. Miyasaka, J. Am. Chem. Soc. 131 (2009) 6050–6051.
[2] H.S. Kim, C.R. Lee, J.H. Im, K.B. Lee, T. Moehl, A. Marchioro, S.J. Moon, R. Humphry-Baker, J.H. Yum, J.E. Moser, et al., Sci. Rep. 2 (2012) 591.
[3] C.R. Kagan, D.B. Mitzi, C.D. Dimitrakopoulos, Science 286 (1999) 945–947 (80-.).
[4] Y. Wang, T. Gould, J.F. Dobson, H. Zhang, H. Yang, X. Yao, H. Zhao, Phys. Chem. Chem. Phys. 16 (2014) 1424–1429.
[5] W.-J. Yin, T. Shi, Y. Yan, Appl. Phys. Lett. 104 (2014) 63903.
[6] T.-Y. Yang, G. Gregori, N. Pellet, M. Grätzel, J. Maier, Angew. Chem. Int. Ed. 54 (2015) 7905–7910.
[7] G. Gregori, T.-Y. Yang, A. Senocrate, J. Maier, M. Grätzel, J. Maier, N.-G. Park, M. Graetzel, T. Miyasaka (Eds.), Org. Halide Perovskite Photovoltaics, Springer International Publishing, Cham, 2016, pp. 107–135.
[8] A. Senocrate, I. Moudrakovski, G.Y. Kim, T.-Y. Yang, G. Gregori, M. Grätzel, J. Maier, Angew. Chem. Int. Ed. 56 (2017) 7755–7759.
[9] C. Eames, J.M. Frost, P.R.F. Barnes, B.C. O'Regan, A. Walsh, M.S. Islam, Nat. Commun. 6 (2015) 7497.
[10] J. Haruyama, K. Sodeyama, L. Han, Y. Tateyama, J. Am. Chem. Soc. 137 (2015) 10048–10051.
[11] S. Meloni, T. Moehl, W. Tress, M. Franckevičius, M. Saliba, Y.H. Lee, P. Gao, M.K. Nazeeruddin, S.M. Zakeeruddin, U. Rothlisberger, et al., Nat. Commun. 7 (2016) 10334.
[12] C. Li, S. Tscheuschner, F. Paulus, P.E. Hopkinson, J. Kießling, A. Köhler, Y. Vaynzof, S. Huettner, Adv. Mater. 28 (2016) 2446–2454.
[13] H. Yu, H. Lu, F. Xie, S. Zhou, N. Zhao, Adv. Funct. Mater. 26 (2016) 1411–1419.
[14] J.M. Azpiroz, E. Mosconi, J. Bisquert, F. De Angelis, Energy Environ. Sci. 8 (2015) 2118–2127.
[15] Y. Yuan, Q. Wang, Y. Shao, H. Lu, T. Li, A. Gruverman, J. Huang, Adv. Energy Mater. 6 (2016) 1501803.
[16] A. Buin, P. Pietsch, J. Xu, O. Voznyy, A.H. Ip, R. Comin, E.H. Sargent, Nano Lett. 14 (2014) 6281–6286.
[17] A. Walsh, D.O. Scanlon, S. Chen, X.G. Gong, S.-H. Wei, Angew. Chem. Int. Ed. 54 (2015) 1791–1794.
[18] Y. Yuan, J. Chae, Y. Shao, Q. Wang, Z. Xiao, A. Centrone, J. Huang, Adv. Energy Mater. 5 (2015) 1500615.
[19] T. Leijtens, E.T. Hoke, G. Grancini, D.J. Slotcavage, G.E. Eperon, J.M. Ball, M. De Bastiani, A.R. Bowring, N. Martino, K. Wojciechowski, et al., Adv. Energy Mater. 5 (2015) 1500962.
[20] J. Mizusaki, K. Arai, K. Fueki, Solid State Ionics 11 (1983) 203–211.
[21] K. Yamada, K. Isobe, E. Tsuyama, T. Okuda, Y. Furukawa, Solid State Ionics 79 (1995) 152–157.
[22] K. Yamada, K. Isobe, T. Okuda, Y. Furukawa, Z. Naturforsch. A 49 (1994) 258–266.
[23] E.J. Juarez-Perez, R.S. Sanchez, L. Badia, G. Garcia-Belmonte, Y.S. Kang, I. Mora-Sero, J. Bisquert, J. Phys. Chem. Lett. 5 (2014) 2390–2394.
[24] H.J. Snaith, A. Abate, J.M. Ball, G.E. Eperon, T. Leijtens, N.K. Noel, S.D. Stranks, J.T.-W. Wang, K. Wojciechowski, W. Zhang, J. Phys. Chem. Lett. 5 (2014) 1511–1515.
[25] V.W. Bergmann, S.A.L. Weber, F. Javier Ramos, M.K. Nazeeruddin, M. Grätzel, D. Li, A.L. Domanski, I. Lieberwirth, S. Ahmad, R. Berger, Nat. Commun. 5 (2014).
[26] O. Almora, A. Guerrero, G. Garcia-Belmonte, Appl. Phys. Lett. 108 (2016) 43903.
[27] B. Chen, M. Yang, X. Zheng, C. Wu, W. Li, Y. Yan, J. Bisquert, G. Garcia-Belmonte, K. Zhu, S. Priya, J. Phys. Chem. Lett. 6 (2015) 4693–4700.
[28] Y. Zhao, C. Liang, H. min Zhang, D. Li, D. Tian, G. Li, X. Jing, W. Zhang, W. Xiao, Q. Liu, et al., Energy Environ. Sci. 8 (2015) 1256–1260.
[29] J. Jamnik, J. Maier, Ber. Bunsenges. Phys. Chem. 101 (1997) 23–40.
[30] J. Jamnik, J. Maier, J. Phys. Chem. Solids 59 (1998) 1555–1569.
[31] J. Maier, Physical Chemistry of Ionic Materials, John Wiley & Sons, Ltd, Chichester, UK, 2004.
[32] J. Maier, Angew. Chem. Int. Ed. 32 (1993) 313–335.
[33] F.A. Kröger, The Chemistry of Imperfect Crystals, North-Holland Publishing Company, Amsterdam, 1964.
[34] G. Brouwer, Philips Res. Rep. 9 (1954) 366–376.
[35] A. Senocrate, T. Acartürk, G. Y. Kim, R. Merkle, U. Starke, M. Grätzel, J. Maier, (Submitted), 2018.
[36] I. Yokota, J. Phys. Soc. Jpn. 16 (1961) 2213–2223.
[37] C.C. Stoumpos, C.D. Malliakas, M.G. Kanatzidis, Inorg. Chem. 52 (2013) 9019–9038.
[38] Q. Dong, Y. Fang, Y. Shao, P. Mulligan, J. Qiu, L. Cao, J. Huang, Science 347 (2015) 967–970 (80-.).
[39] R. Merkle, J. Maier, Angew. Chem. Int. Ed. 47 (2008) 3874–3894.
[40] J. Maier, Phys. Chem. Chem. Phys. 5 (2003) 2164–2173.
[41] J.-H. Im, C.-R. Lee, J.-W. Lee, S.-W. Park, N.-G. Park, Nanoscale 3 (2011) 4088–4093.
[42] M.I. Saidaminov, A.L. Abdelhady, B. Murali, E. Alarousu, V.M. Burlakov, W. Peng, I. Dursun, L. Wang, Y. He, G. Maculan, et al., Nat. Commun. 6 (2015) 7586.